Journal of Applied Polymer Science

In situ electrochemical synthesis of a poly(*o*-anisidine) counter electrode for a dye-sensitized solar cell

Chandrasekaran Menaka, Paramasivam Manisankar, Thambusamy Stalin
Photoelectrochemistry Laboratory, Department of Industrial Chemistry, Alagappa University, Karaikudi 3, Tamilnadu, India
Correspondence to: T. Stalin (E-mail: drstalin76@gmail.com)

ABSTRACT: Poly(*o*-anisidine) (POA) counter electrodes (CEs) were fabricated by potentiodynamic deposition and incorporated into platinum (Pt)-free dye-sensitized solar cells (DSSCs). A different sweep number had great impact on the morphology and electrocatalytic activity of the POA films. The POA film fabricated by 25 sweep cycles was observed to have a highly porous morphology, and this resulted in a lower charge-transfer resistance of 57 cm^2 in comparison with the Pt CE. The DSSC assembled with the POA CE showed a higher photovoltaic conversion efficiency of 1.67% compared to 1.2% for the DSSC with the Pt CE under full sunlight illumination. Therefore, the high active surface area of the 25-sweep-segmented POA film could be considered a promising alternative CE for use in DSSCs because of its high electrocatalytic performance and electrochemical stability. © 2015 Wiley Periodicals, Inc. J. Appl. Polym. Sci. **2015**, *132*, 42041.

KEYWORDS: applications; conducting polymers; electrochemistry; spectroscopy

Received 14 November 2014; accepted 25 January 2015
DOI: 10.1002/app.42041

INTRODUCTION

Until recently, research and development efforts have been intensified to find new renewable sources because of the alarming position of fossil fuels. The abundance of easily accessible solar radiation has implemented cost-effective solar-cell technologies for the growth of energy sources. Solar cells directly convert solar energy into electrical energy, and they are able to produce electricity without special maintenance and environmental concerns.[1] Dye-sensitized solar cells (DSSCs) have emerged as a viable alternative because of their low cost, good durability, and high-energy conversion efficiency.[2] A typical DSSC sandwiches a liquid electrolyte containing iodide/triiodide (I^-/I_3^-) redox couples between a photo anode comprising TiO_2 nanocrystals sensitized by dye molecules and a CE.[3] The CE plays a crucial role as an electron charge carrier from the external circuit to the redox electrolyte.

Platinum (Pt) is a preferred CE material for the reduction reaction of redox couples because of its superior electrocatalytic activity and stability. However, the high cost of Pt has prevented it from being widely used in commercial DSSCs. The reflection of its chemical stability and cost effectiveness is necessary in the development of a new class of catalyst that contains a reduced Pt content yet provides an improved redox reaction efficiency, good chemical stability, sustained lifetime, reduced manufacturing cost, and abundant and cheap feedstock.[4] Carbon materials[5] and conducting polymers[6] are believed as an efficient material for Pt. It has been proven that poly(*o*-anisidine) (POA) as a potential replacement for Pt. The need for new materials with potential properties has always been the driving power for progress in science and technology. The incorporation of constituents in the polymer skeleton is a common technique for synthesizing polymers having improved properties.[7,8]

For this purpose, we put into a new step to perform with a derivative of aniline, an methoxy substituted at the o position (*o*-anisidine) as a CE material. The choice of *o*-anisidine as the monomer for this study was based on the following: (1) the methoxy (—OCH_3) substituent groups present in the backbone of the polymer causes a decrease in the stiffness of the polymer chain and results in more salvation, (2) the monomer *o*-anisidine is commercially available at low cost, and (3) the product has a more regular structure consequently, and this leads to higher polymerization yields.[9,10]

Unfortunately, the use of POA for its application as a CE material for DSSCs have not yet been explored. In this study, we examined a facile layer-by-layer self-assembly process to generate POA conducting multilayer CEs with good electrochemical properties for applications in DSSCs. Moreover, the effect of the sweep number and the thickness, surface morphology, electrocatalytic activity, and efficiency of the POA deposit CE were studied.

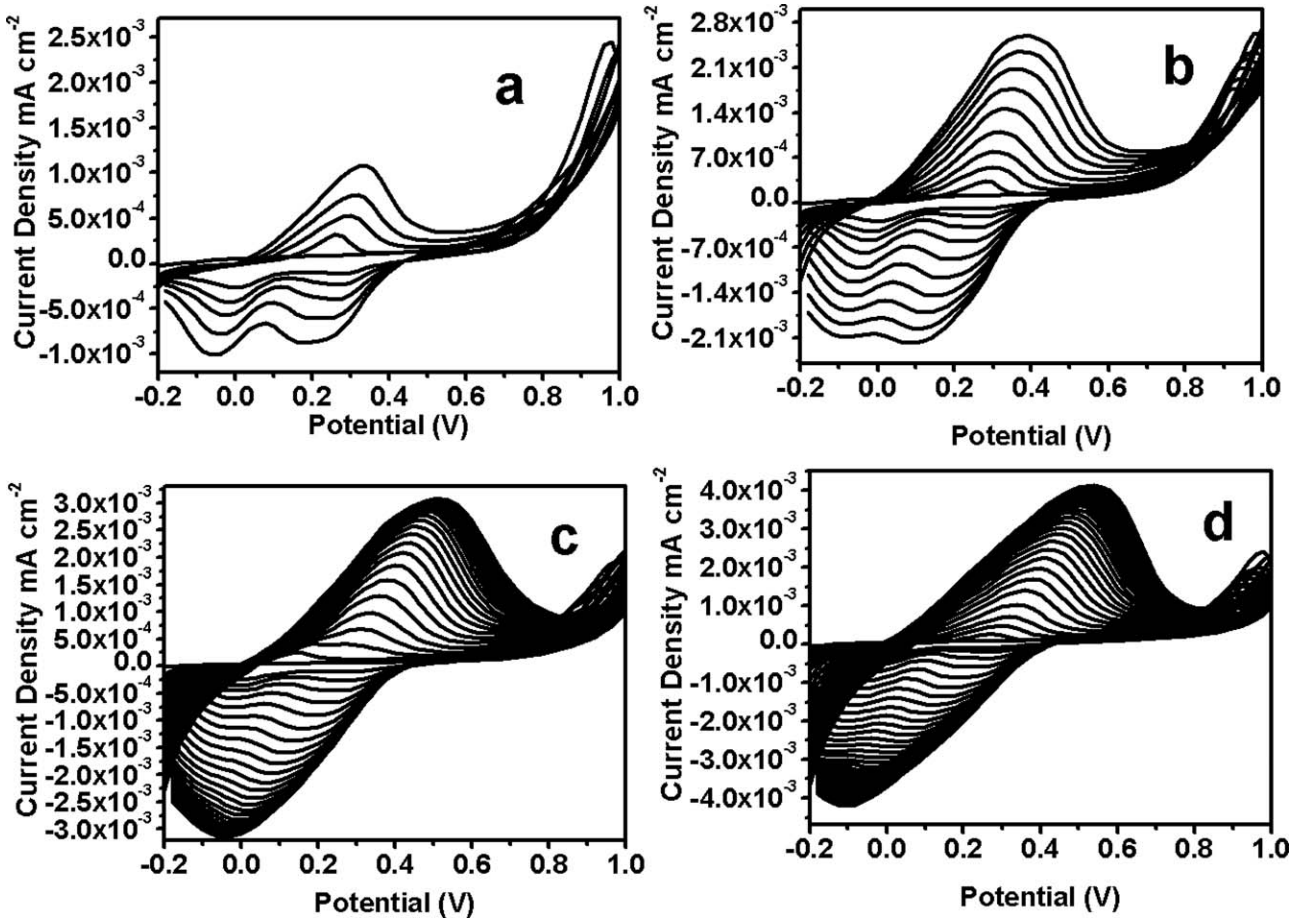

Figure 1. Electrodeposition in various sweep segments of POA by cyclic voltammetry on an SS plate: (a) 5, (b) 10, (c) 25, and (d) 50 cycles.

EXPERIMENTAL

Materials

o-Anisidine (SD Fine) was vacuum-distilled before use. sulfuric acid (Merck), $LiClO_4$ (Alfa Aesar), LiI (Alfa Aesar), and I_2 (SRL, Ltd.) were used as received. All other chemicals and solvents were analytical grade and were used as received.

A stainless steel 304 plate was rinsed with deionized water, immersed in ethanol and acetone, and ultrasonically treated for 15 min before electropolymerization. The deposited area was 1 cm^2, with the other area insulated by adhesive tape. POA was electropolymerized on the surface of stainless steel (SS) by the cyclic voltammetry method. For electropolymerization, an aqueous solution of 0.1*M* *o*-anisidine and 0.1*M* H_2SO_4 was prepared. An SS sheet was used as the working electrode in the three-electrode system (Pt wire auxiliary electrode and Ag/AgCl reference electrode), and it was immersed in the previous solutions. Cyclic voltammetric studies were carried out with an Autolab electrochemical work station. We deposited POA films with various thicknesses by controlling the number of cycles, which were 5, 10, 25, and 50 with a scan rate of 100 mV/s, between −0.2 and 1 V. The coated POA films were rinsed with 0.1*M* H_2SO_4 to remove soluble monomeric species.

Characterization of the Electrode

The surface morphologies of the prepared membranes were inspected by scanning electron microscopy (SEM) with an SCi-QuantaFEG 250 instrument high resolution scanning electron microscope (HRSEM). Polymerization experiments and cyclic voltammogram measurements were performed on an

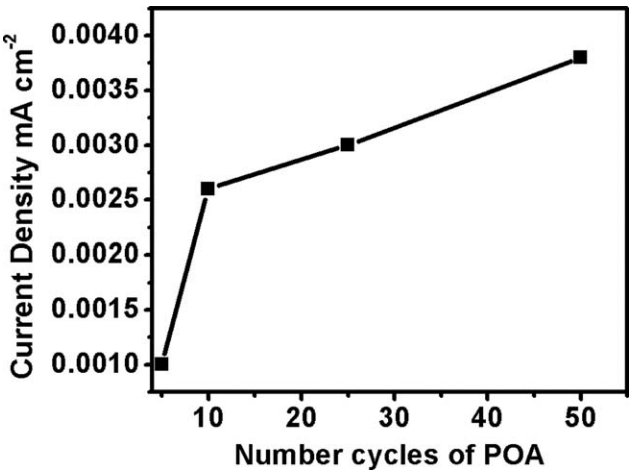

Figure 2. Current enhancement during the cyclic voltammetry growth of 25-sweep-segmented POA.

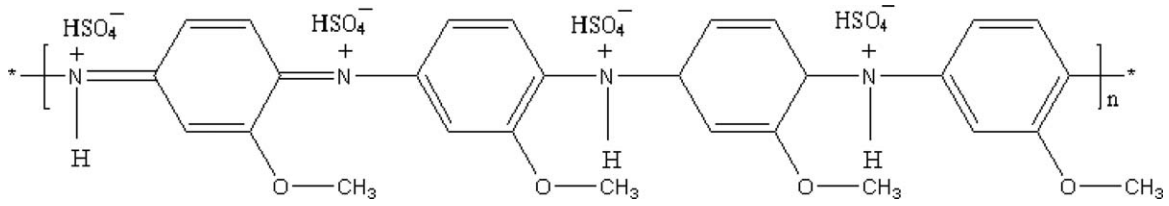

Figure 3. Molecular structure of POA.

Autolab PGSTAT 30 (EcoChemi, The Netherlands). For cyclic voltammogram studies, three-electrode systems were used. For this, POA/SS, Pt-foiled, and saturated calomel electrodes were used as working, counter, and reference electrodes, respectively. The electrolyte was an acetonitrile solution containing 0.01*M* LiI, 0.001*M* I_2, and 0.1*M* $LiClO_4$. The electrochemical impedance spectroscopy (EIS) measurement of POA/SS films were performed in a three-electrode cell with an Autolab PGSTAT 30 (EcoChemi, The Netherlands) in the frequency range 0.1–10^5 Hz. The magnitude of the alternative signal was 5 mV.

Fabrication of the DSSC Device

The fluorine-dopped tin oxide (FTO) glass substrate were cleaned with deionized water and anhydrous ethanol and ultrasound for 15 min. The TiO_2 slurry was prepared by the vigorous grinding of 2 mL of an aqueous poly(ethylene glycol) solution with 0.5 g of TiO_2 powder. The thin films of TiO_2 (P25 Degussa) were produced by a doctor blade technique from a colloidal paste of TiO_2; this was followed by a sintering step at 450°C for 30 min. The thickness of the TiO_2 film was about 10 μm. The TiO_2 film was preheated at 120°C for 30 min and then immersed into 0.3 m*M* Rose Bengal in ethanol overnight. Afterward, the electrode was washed with ethanol and then dried in air. The sandwich-type solar cells consisted of a dye-sensitized TiO_2 film as a working electrode, POA as CE, and an electrolyte containing 0.5*M* LiI, 0.05*M* I_2, and 0.5*M* *t*-butyl pyridine in an acetonitrile solution. Last, the sandwich-type DSSC was fabricated by the clamping of the CE on top of the TiO_2 photoelectrode, and an electrolyte was inserted and sealed.

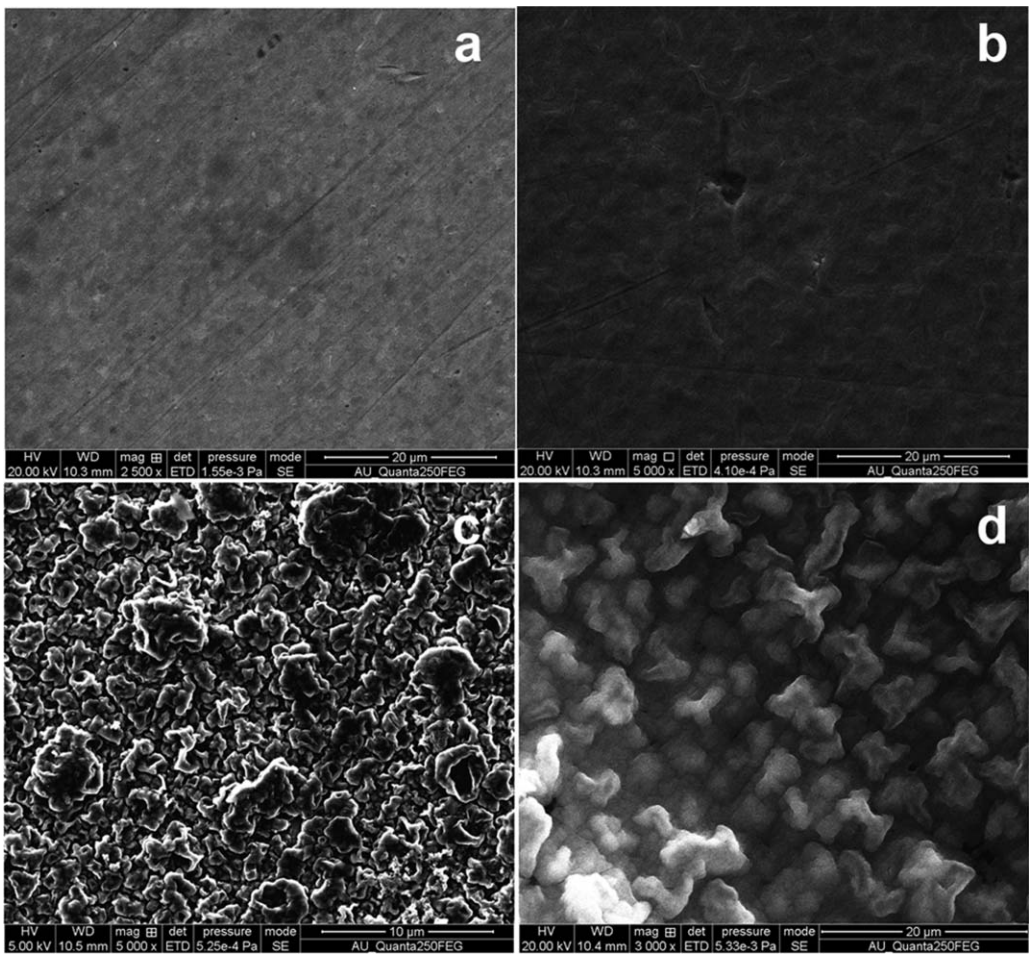

Figure 4. SEM images of the CE materials: POA deposits prepared with (a) 5, (b) 10, (c) 25, and (d) 50 sweep cycles.

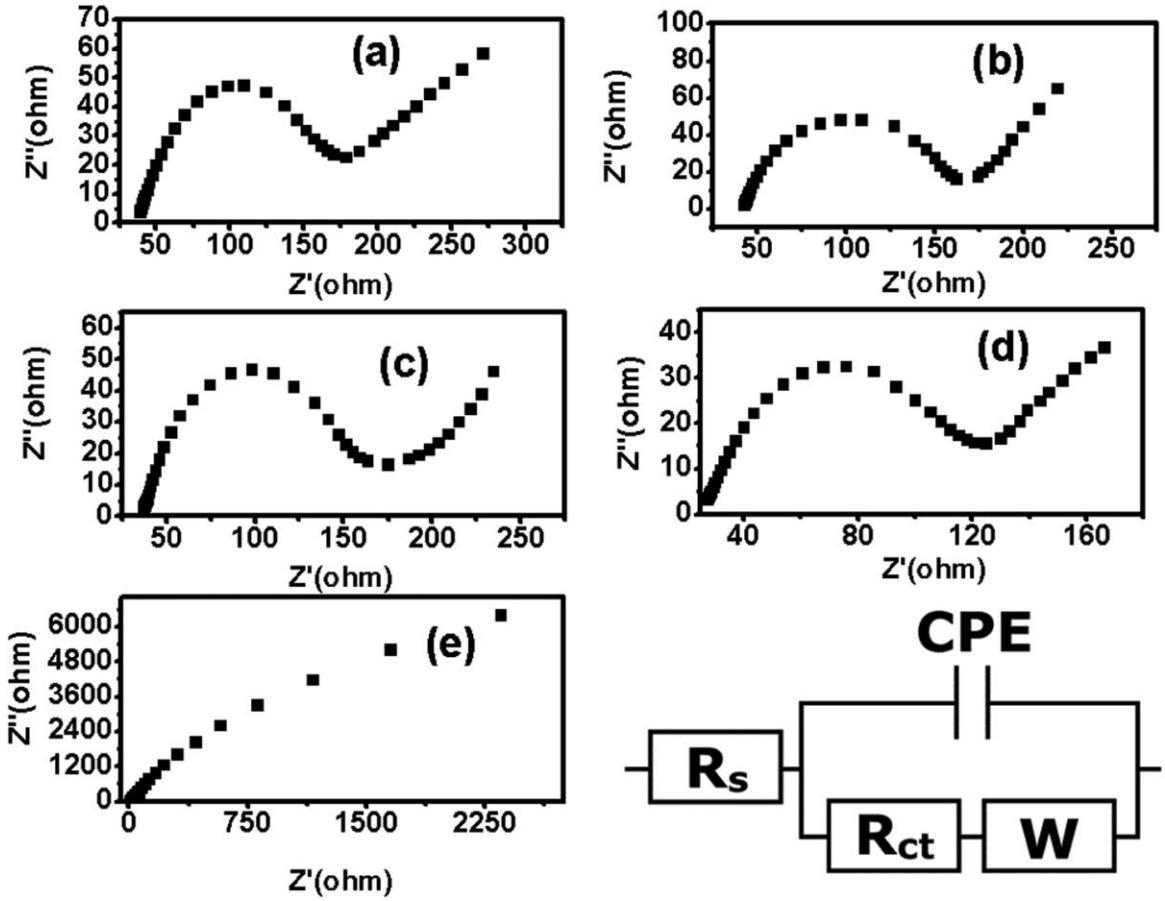

Figure 5. Impedance spectra of the (a) 5-, (b) 10-, (c) 50-, and (d) 25-sweep-segmented POA and (e) SS plate and (f) equivalent circuit. Z″ = imaginary part; Z′ = real part; CPE = constant phase element.

RESULTS AND DISCUSSION

Synthesis of POA CEs

Figure 1(a–d) shows the cyclic voltammogram recorded synthesis of POA at different sweep numbers on the SS plate surface. During the deposition of the POA film, the oxidation and reduction peaks were recorded on a forward and reverse potential scan. The growth of the polymer took place layer by layer, and each layer became electrochemically active before the next layer was deposited. The presence of an electron-releasing group in the ortho position much favors the electropolymerization of *o*-anisidine. Patil *et al.*[11] found better POA growth when it was electrosynthesized with the potentiodynamic method. The anodic peak was assigned to the oxidation of POA deposited at the electrode surface corresponding to the conversion of amine units into radical cations.

Table I. Best Fit Values for R_s and R_{ct} of the Equivalent Circuit Shown in Figure 4(f)

POA sweep segment	R_s (ohm cm^2)	R_{ct} (ohm cm^2)
05	36	69
10	42	66
25	26	57
50	37	61

Figure 2 correlates the relation between the number of cycles and the peak current. The peak current density (i_p) increased with the number of cycles; this indicated the formation of conducting polymer films in each case.[12] In each cycle, the deposition of electroactive POA increased, and this led to an increase in the current. The current increased with increasing number of

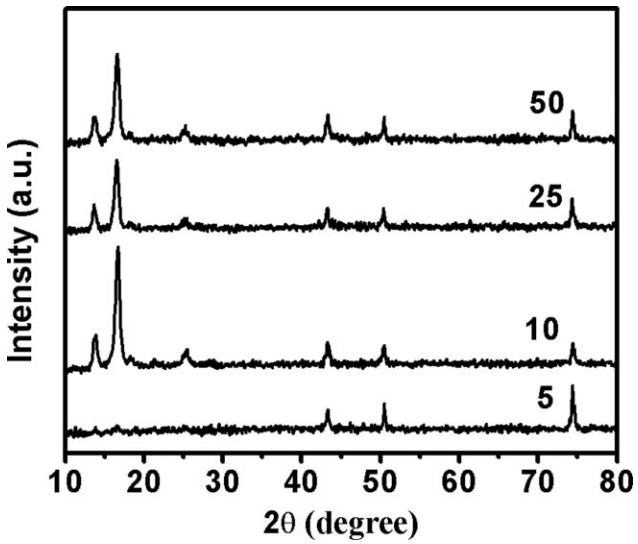

Figure 6. X-ray diffraction pattern of the POA CEs.

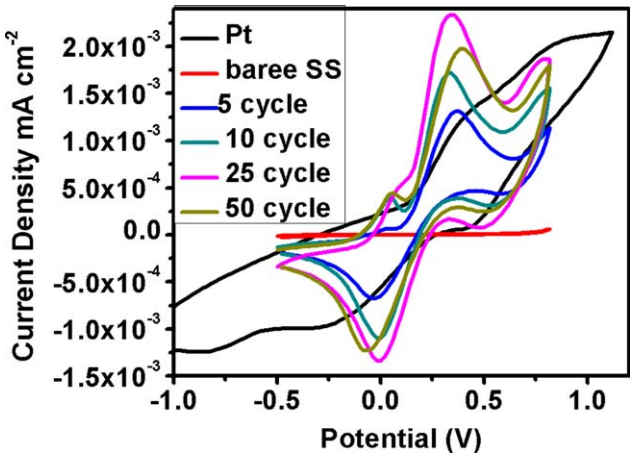

Figure 7. Cyclic voltammogram of the POA and Pt CEs. [Color figure can be viewed in the online issue, which is available at www.interscience.wiley.com.]

sweep segments; this indicated progressive polymerization and film growth. The molecular structure of the POA chain is shown in Figure 3.

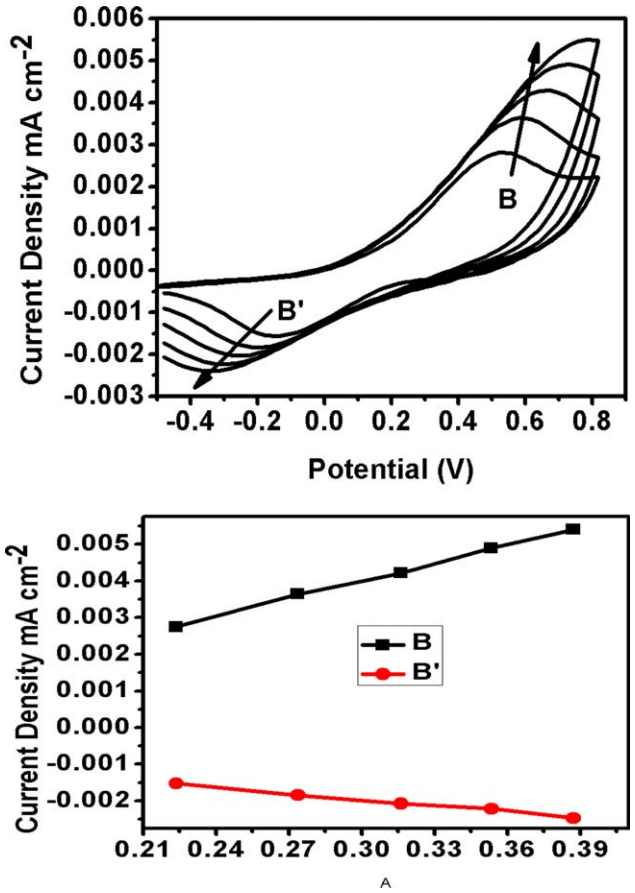

Figure 8. (a) Cyclic voltammogram for the 25-sweep-segmented POA CEs with scan rates of 50, 75, 100, and 125 (from the inside to the outside) and the (b) relationship between the redox peak current and scan rate. B = oxidation peak current density; B′ = reduction peak current density of the counter electrode. [Color figure can be viewed in the online issue, which is available at www.interscience.wiley.com.]

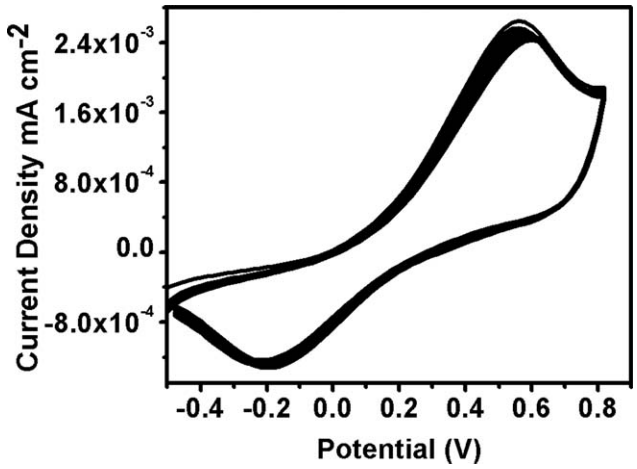

Figure 9. Cyclic voltammogram of the POA CEs (10 consecutive cycles).

Surface Morphology of the POA Film

The surface morphology of POA CE is shown in Figure 4. The SEM images in Figure 4(a,b) (5th and 10th sweep segment) show that the POA synthesis showed very low polymerization growth on the surface. The 25 sweep segments of POA in Figure 3(c) showed some spongelike morphology, which indicated a high surface area. The rough and large surface area shown in Figure 4(c) provided a massive number of active sites for the movement of iodide redox couple electrolytes[13] into the electrode surface, and it could lead to an elevation of the current density of the DSSCs. As shown in Figure 4(d), the 50-sweep segmented POA had an irregular flakelike structure because of the decreased active surface area because of the higher number of polymerization cycles.

Impedance Analysis

The Nyquist plot in Figure 5 illustrates the impedance characteristics of the POA CEs. According to the equivalent circuit, the intercept on the real axis represents the series resistance (R_s), a reflection of film resistance. The arc in the high-

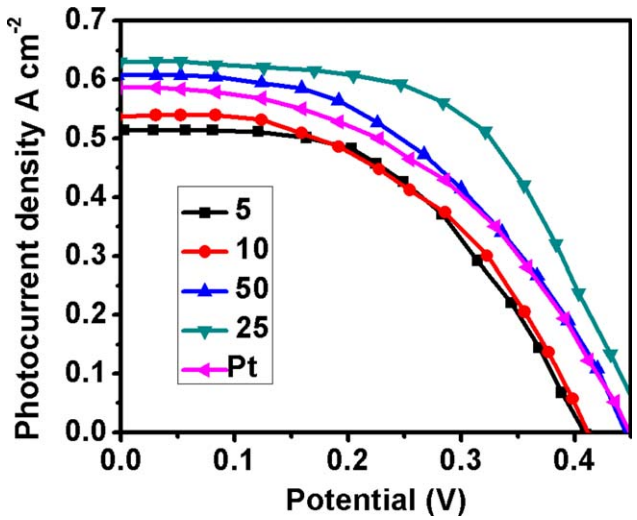

Figure 10. Density–voltage curves of the DSSCs based on POA and Pt CEs. [Color figure can be viewed in the online issue, which is available at www.interscience.wiley.com.]

Table II. Photovoltaic Parameters of the DSSCs Based on Pt and POA CEs

CE	J_{sc} (A/cm^2)	V_{oc} (V)	Fill factor	η (%)
Pt	0.5869	0.4560	0.51	1.38
5	0.51	0.42	0.47	1.03
10	0.53	0.42	0.51	1.10
25	0.63	0.49	0.53	1.67
50	0.61	0.46	0.53	1.52

η = efficiency of the cell.

frequency region arose because of the charge-transfer resistance (R_{ct}) at the CE/electrolyte interface; this changed inversely with the electrocatalytic activity of the CEs on the reduction of triiodide, whereas W is the diffusion resistance of the I^-/I_3^- redox species.[14]

Table I shows the impedance parameters obtained from the equivalent circuit from Figure 5. Because of the symmetric configuration of the dummy cell, the real R_{ct} value was calculated as half of the value obtained. As shown in the table, both R_s and R_{ct} decreased with increasing sweep segment; this indicated an inverse order of electrocatalytic activity. After a certain thickness was achieved, the effect was reversed. The R_{ct} of the 25-sweep-segmented POA guided the fast electron transfer at the junction between the CE and the electrolyte.[15] Moreover, W of I^-/I_3^- decreased for the 25th sweep segment. This was because the lower deposition cycle could not produce enough catalytic active sites, and a higher sweep number generated an increased film thickness and resistance for charge transfer.

X-ray Diffraction Analysis

The X-ray diffraction pattern of the synthesized CEs is shown in Figure 6. In the X-ray diffraction pattern, there were reflections at 45, 52, and 75 corresponding to the SS plate.[16] For POA, a broad peak occurring at $2\theta \approx 25.6$ was amorphous in nature and could be ascribed to the periodicity parallel and perpendicular to the polymer chains of POA.[17]

Electrical Properties of the CEs

For further confirmation of the results from the SEM and EIS analyses, cyclic voltammetric tests were conducted. It is well-known that the reaction occurring on the CE of the DSSCs is

$$3I^- - 2e^- I_3^- \text{ Anodic peak} \quad (1)$$

$$I_3^- + 2e^- 3I^- \text{ Cathodic peak} \quad (2)$$

In this interval, the anodic peak is contributed by eq. (1) in an anodic sweep, and the cathodic peak is contributed by eq. (2) in a cathodic sweep, respectively. Consequently, only the cathodic reaction is considered in the cyclic voltammogram test.[18]

Moreover, the cathodic i_p of the 25-sweep-segmented POA CE was significantly higher than the other POA CE, as shown in Figure 7. This indicated that a much faster reaction rate for I^-/I_3^- reaction was demonstrated. We concluded that when the thickness of the film increased, the catalytic activity increased, attained a maximum value, and after that the value, decreased. This was because the shorter deposition time could not produce enough catalytically active sites and the longer deposition time generated an increased film thickness and resistance for charge transfer. Increased torsional angles brought about by the substituent groups resulted in a decrease in the orbital overlap of the π electrons and nitrogen lone pairs; this was likely the reason for the increased catalytic behavior.[19]

Figure 8(a) illustrates the relationship between the redox i_p of POA and the square root of the scan rate in acetonitrile solution. Both the cathodic and anodic i_p increased approximately linearly and were proportional to the square root of the scan rate. A good linear relationship of 25th sweep segment of POA indicated that the redox reaction of I^-/I_3^- on electrodes was controlled by the ionic diffusion of the electrolyte and indicated an adsorption-controlled electrode process; this was related to the transport of iodide species inside the POA film and in the bulk solution.[20] The linearity of the i_p values with the square root of the scan rate in Figure 8(b) indicated that charge transfer in the redox step was empirically controlled by the diffusion of charges in the films as described by Randles–Sevcik theory:[21]

$$i_p = \left(2.69 \times 10^5\right) n^{3/2} C^b A D^{1/2} v^{1/2}$$

where n is the number of electrons, A is the surface area of the electrode (cm^2), D is the diffusion constant (cm^2/s), C^b is the bulk concentration of electroactive species (mol/cm^3), and v is the scan rate (V/s). Therefore, for the diffusion-controlled process, the peak current was proportional to the square root of the scan rate. In the consecutive 10-cycle test, the cyclic voltammograms did not change and exhibited stable anodic i_p and cathodic i_p (Figure 9); this indicated good uniformity and excellent electrochemical stability in the 25-cycled POA CE film on the SS substrate.

Photovoltaic Performances

Figure 10 shows the photocurrent density–voltage responses of the DSSCs with the POA CEs, and Table II shows their photovoltaic parameters. The DSSC with the 25-sweep-cycle POA CE had the highest short-circuit photocurrent density ($J_{sc} = 0.63$ mA/cm^2), open-circuit voltage ($V_{oc} = 0.49$ V), and fill factor (0.53) and provided a good photovoltaic conversion efficiency (PCE) of 1.67%. This PCE and other solar-cell parameters were superior to those of the Pt and POA CEs. CEs made by higher sweep cycles led to a decrease in J_{sc} and PCE because of an increase in the internal resistance that resulted from the inappropriate thickness (POA) of the CEs

CONCLUSIONS

We fabricated POA CEs by the potentiodynamic deposition and their Pt-free DSSCs. The POA CE with 25 sweep segments was more electrochemically active and showed a higher PCE; this was due to the appropriate polymer growth and active surface area (SEM), which enhanced the rate of I^-/I_3^- redox reaction. The lower R_{ct} value of the CE/electrolyte interface implied a facile electron transfer from CE to I_3^- ions compared to the other CEs. Therefore, we concluded that the different sweep cycle scans impacted the morphology of the POA films, and this affected the electrocatalytic performance of the I^-/I_3^- redox reaction, J_{sc}, and PCE of the DSSC.

ACKNOWLEDGMENTS

One of the authors (T.S.) is thankful to the University Grants Commission (New Delhi, India) for its financial support through the Major Research Project Fund [File Number 40-72/2011(SR), 2011).

REFERENCES

1. Gratzel, M. J. *Photochem. Photobiol. A* **2004**, *164*, 3.
2. Jihuai, W.; Yan, L.; Qunwei, T.; Gentian, Y.; Jianming, L.; Miaoliang, H.; Lijian, M. *Sci. Rep.* **2014**, *4*, 1.
3. Xiaoxu, C.; Qunwei, T.; Benlin, H. *Mater. Lett.* **2014**, *119*, 28.
4. Ganapathy, V.; Karunagaran, B.; Shi-Woo, R. *ACS Appl. Mater. Interfaces* **2011**, *3*, 857.
5. Lee, K. M.; Chiu, W.-H.; Wei, H.-Y.; Hu, C.-W.; Suryanarayanan, V.; Hsieh, W.-F.; Ho, K.-C. *Thin Solid Films* **2010**, *518*, 1716.
6. Lin, Z. P.; Ye, B. X.; Hu, X. D.; Ma, X. Y.; Zhang, X. P.; Deng, Y. Q. *Electrochem. Commun.* **2009**, *11*, 1768.
7. Mattoso, L. H. C.; Bilhoes, L. O. S. *Synth. Met.* **1992**, *52*, 171.
8. Mattoso, L. H. C.; Manoher, S. K.; MacDiarmid, A. G.; Epstein, A. *J. Polym. Sci. Part A: Polym. Chem.* **1995**, *33*, 1227.
9. Valle, M. A.; Manuel, A. E.; Borrego, D.; Pedro, P. Z.; Fernando, R.; Díaz1, Maria, B. C.; Mónica, P. A.; Juan, P. S. *Int. J. Electrochem. Sci.* **2012**, *7*, 2552.
10. Leclerc, M.; Guay, J.; Dao, L. H. *J. Electroanal. Chem.* **1988**, *251*, 21.
11. Sharmila, P.; Mahajan, J. R.; More, M. A.; Patil, P. P.; Gosavi, S. W.; Ganga, S. *Polym. Int.* **1998**, *46*, 99.
12. Borole, D. D.; Kapadi, U. R.; Mahulikar, P. P.; Hundiwale, D. G. *Polym. Plast. Technol. Eng.* **2006**, *45*, 667.
13. Li, Q.; Wu, J.; Tang, Q.; Lan, Z.; Li, P.; Lin, J.; Fan, L. *Electrochem. Commun.* **2008**, *10*, 1299.
14. Qiu, Y.; Lu, S.; Wang, S.; Zhang, X.; He, S.; He, T. *J. Power Sources* **2014**, *253*, 300.
15. Niu, L.; Li, Q.; Wei, F.; Chen, X.; Wang, H. *J. Electroanal. Chem.* **2003**, *544*, 121.
16. Leoni, M.; Scardi, P.; Rossi, S.; Fedrizzi, L.; Massiani, Y. *Thin Solid Films* **1999**, *345*, 263.
17. Zhang, L.; Peng, H.; Sui, J.; Soeller, C.; Kilmartin, P. A.; Sejdic, J. T. *J. Phys. Chem. C* **2009**, *113*, 9128.
18. Lin, J. Y.; Lia, J. H.; Chou, S. W. *Electrochim. Acta* **2011**, *56*, 8818.
19. Wang, S.; Lu, S.; Li, X.; Zhang, X.; He, S.; He, T. *J. Power Sources* **2013**, *242*, 438.
20. Xiao, Y. M.; Lin, J. Y.; Tai, S. Y.; Chou, S. W.; Yue, G. T.; Wu, J. H. *J. Mater. Chem.* **2012**, *22*, 19919.
21. Lee, K. M.; Hsu, C. Y.; Chen, P. Y.; Ikegami, M.; Miyasaka, T.; Ho, K. C. *Phys. Chem. Chem. Phys.* **2009**, *11*, 3375.